Dynamical sweet and sour regions in bichromatically driven Floquet qubits

D. Dominic Briseño-Colunga,[1,*] Bibek Bhandari,[1,*,†] Debmalya Das,[2,3] Long B. Nguyen,[4,5] Yosep Kim,[6] David I. Santiago,[4,5] Irfan Siddiqi,[4,5] Andrew N. Jordan,[1,7,8,9] and Justin Dressel[1,7]

[1] *Institute for Quantum Studies, Chapman University, Orange, California 92866, USA*
[2] *Dipartimento di Fisica, Università di Bari, I-70126 Bari, Italy*
[3] *INFN, Sezione di Bari, I-70125 Bari, Italy*
[4] *Quantum Nanoelectronics Laboratory, Department of Physics, University of California, Berkeley, California 94720, USA*
[5] *Applied Mathematics and Computational Research Division, Lawrence Berkeley National Laboratory, Berkeley, California 94720, USA*
[6] *Department of Physics, Korea University, Seoul 02841, Korea*
[7] *Schmid College of Science and Technology, Chapman University, Orange, California 92866, USA*
[8] *The Kennedy Chair in Physics, Chapman University, Orange, California 92866, USA*
[9] *Department of Physics and Astronomy, University of Rochester, Rochester, New York 14627, USA*

(Received 3 June 2025; revised 29 September 2025; accepted 23 December 2025; published 30 January 2026)

Modern superconducting and semiconducting quantum hardware uses external charge and microwave flux drives to both tune and operate devices. However, each external drive is susceptible to low-frequency (e.g., $1/f$) noise that can drastically reduce the coherence time of the device unless the drive is placed at specific operating points that minimize the sensitivity to fluctuations. We show that operating a qubit in a driven frame using two periodic drives of distinct commensurate frequencies can have advantages over both monochromatically driven frames and static frames with constant offset drives. Employing Floquet theory, we analyze the spectral and lifetime characteristics of a two-level system under weak and strong bichromatic drives, identifying drive-parameter regions with high coherence ("sweet spots") and highlighting regions where coherence is limited by additional sensitivity to noise at the drive frequencies ("sour spots"). We present analytical expressions for quasienergy gaps and dephasing rates, demonstrating that bichromatic driving can alleviate the trade-off between dc and ac noise robustness observed in monochromatic drives. This approach reveals continuous manifolds of doubly dynamical sweet spots, along which drive parameters can be varied without compromising coherence. Our results motivate further study of bichromatic Floquet engineering as a powerful strategy for maintaining tunability in high-coherence quantum systems.

DOI: 10.1103/5dmn-yjq5

I. INTRODUCTION

The pursuit of robust, high-coherence qubits has driven remarkable progress in both superconducting [1–8] and semiconducting quantum platforms [9–14]. Superconducting qubits, while offering good controllability and scalability [15,16], are more susceptible to environmental noise and decoherence, leading to shorter coherence times [5,10]. In contrast, semiconducting spin qubits leverage atomic scale confinement and material isolation to achieve significantly longer coherence times [17–20], though their control and scalability remain technically challenging [18,21]. However, both platforms face a critical challenge: decoherence induced by low-frequency noise [1,5,6,10,18,22–26]. For superconducting flux-tunable qubits, ubiquitous $1/f$ flux noise limits their static (undriven) operation to particular flux bias choices that minimize noise sensitivity, restricting tunability [24,27–29]. Similarly, semiconducting spin qubits are susceptible to low-frequency noise in either electric charge or magnetic flux (depending on the design), as well as decoherence from coupling to phonon baths [18,29]. This necessitates dynamic error-suppression strategies such as spin-echo or dynamical decoupling [30–33].

Recent advances in Floquet engineering—the use of periodic drives to reshape a quantum system's effective Hamiltonian—enable an intriguing approach to addressing these challenges by encoding qubit information in a rotating frame that is dynamically decoupled from the

*These authors contributed equally.
†Contact author: bbhandari@chapman.edu

low-frequency noise [6,27,28,34]. In superconducting circuits, replacing static flux (charge) bias with periodic monochromatic flux (charge) drives has revealed dynamical sweet spots with enhanced noise resilience, enabling high-fidelity gates [6,8,28,35,36]. Parallel developments in semiconductor qubits have exploited periodic driving to suppress charge noise via spin-locking [10–14,24] and dynamical decoupling from spin baths [18,30,37]. These successes highlight a cross-platform principle: periodic drives can help decouple qubits from low-frequency noise while allowing control. However, existing strategies in both domains face limitations as monochromatic drives restrict parameter manifolds [24].

Bichromatic driving has recently emerged as a promising strategy for noise-resilient quantum control [27,38]. Recent experiments in superconducting circuits leveraged bichromatic drives to create continuous dynamical sweet spots, enabling high-fidelity single- and two-qubit gates [27]. Furthermore, in Ref. [6], bichromatic driving was employed to suppress static *ZZ* coupling between Floquet qubits, helping realize a high-fidelity two-qubit gate. Building on these advances, we theoretically investigate how bichromatic driving reshapes the qubit-environment interaction, either suppressing or enhancing sensitivity to noise at both low frequencies and the drive frequencies. By studying the interplay between drive-engineered spectral manifolds and environmental coupling, this work establishes design principles for decoherence mitigation in dynamical qubits.

In this paper, we investigate bichromatic Floquet engineering as a strategy for noise-protected qubit operation. Our analytical framework reveals universal features applicable to superconducting and semiconducting spin qubits transversely coupled to a noisy environment. Using a generic two-level system as a testbed (see Sec. I A for the model Hamiltonian and Sec. I B for the noise model), we demonstrate that bichromatic driving creates continuous high-coherence manifolds in parameter space in the weak (see Sec. II A) and beyond the weak-driving regime (see Sec. II B), where decoherence from $1/f$ flux noise is suppressed by orders of magnitude. By deriving analytic expressions for the ac Stark shift using generalized van Vleck (GVV) perturbation theory, we provide a detailed theoretical analysis of the fast-driving regime (see Sec. II C). Our analysis directly connects the gap's sensitivity to external drive parameters, such as the modulation amplitude and drive frequency, enabling precise identification of dynamical regions of low sensitivity to dc and ac noise (doubly sweet spots).

A. Driven two-level system Hamiltonian

We consider the system Hamiltonian (setting $\hbar = 1$) of the form

$$\hat{H}(t) = -\frac{w_q}{2}\hat{\sigma}_{\mathrm{z}} + \frac{d(t)}{2}\hat{\sigma}_{\mathrm{x}}, \tag{1}$$

where the first term on the right-hand side is the undriven qubit Hamiltonian. We define the Pauli operators as $\hat{\sigma}_{\mathrm{z}} = |g\rangle\langle g| - |e\rangle\langle e|$ and $\hat{\sigma}_{\mathrm{x}} = |g\rangle\langle e| + |e\rangle\langle g|$. We parameterize the external drive, $d(t)$, as

$$d(t) = \Omega\cos(\nu)\cos(N_1\omega t) + \Omega\sin(\nu)\cos(N_2\omega t) + b, \tag{2}$$

where b is the dc component of the drive, Ω sets the ac drive strength, and ν is a time-independent mixing angle. We consider commensurate drive frequencies, $N_1\omega$ and $N_2\omega$, by choosing N_1 and N_2 to be integers. We refer to the case where $\Omega = 0$ as a "dc qubit."

A periodically driven Hamiltonian admits orthonormal, quasiperiodic solutions called Floquet states, $|\psi_\pm(t)\rangle = e^{-i\epsilon_\pm t}|u_\pm(t)\rangle$, where $\epsilon_\pm$ is called the quasienergy, and $|u_\pm(t)\rangle$ is the T-periodic Floquet mode for the Floquet states $(+,-)$ (see Appendix A for details). The quasienergies and their respective Floquet modes are eigenvalues and eigenvectors of a Hermitian operator called the Floquet Hamiltonian, $\hat{H}_{\mathrm{F}}(t) = \hat{H}(t) - i(\partial/\partial t)$. The Floquet Hamiltonian is the effective Hamiltonian under periodic driving. The Floquet modes may be expanded as

$$|u_\pm\rangle = \sum_{n,\alpha} c^{\pm}_{n,\alpha}\,|n,\alpha\rangle\,, \tag{3}$$

where $c^{\pm}_{n,\alpha} = (1/T)\int_0^T e^{-in\omega t}\langle\alpha|u_\pm\rangle dt$ are the time-independent Floquet coefficients for the two-level system state $|\alpha\rangle \equiv \{|g\rangle\,,|e\rangle\}$. In Eq. (A4) in Appendix A, we set the basis for the T-periodic functions $(\mathcal{T})$ as $\{|n\rangle = e^{in\omega t}\}_{n\in\mathbb{Z}}$. Furthermore, the state $|n,\alpha\rangle = e^{in\omega t}|\alpha\rangle$ satisfies the properties of a product space between $\mathcal{T}$ and the atomic states of the undriven system. Changing coordinates to the extended Hilbert space determined by the basis $|n,\alpha\rangle$, the Floquet Hamiltonian can be written as $\hat{H}_{\mathrm{F}} = \hat{H}_0 + \hat{H}_{\mathrm{dc}} + \hat{H}_{\mathrm{ac}}$, where $\hat{H}_0$ describes the undriven qubit dynamics, $\hat{H}_{\mathrm{dc}}$ describes the action of the dc bias b plus the operator $-i\partial_t$, and $\hat{H}_{\mathrm{ac}}$ describes the action of the ac drive. They are (see Appendix B)

$$\hat{H}_0 = \hat{1}_{\mathcal{T}} \otimes \left(-\frac{w_q}{2}\hat{\sigma}_{\mathrm{z}}\right), \tag{4}$$

$$\hat{H}_{\mathrm{dc}} = \sum_m |m\rangle\langle m| \otimes \left(m\omega + \frac{b}{2}\hat{\sigma}_{\mathrm{x}}\right), \tag{5}$$

$$\hat{H}_{\mathrm{ac}} = \frac{\Omega}{4}\sum_n (\cos\nu\,|n-N_1\rangle\langle n| + \sin\nu\,|n-N_2\rangle\langle n|)\otimes\hat{\sigma}_{\mathrm{x}} + \mathrm{H.c.}, \tag{6}$$

where $\hat{1}_{\mathcal{T}}$ is the identity operator in the $\mathcal{T}$ space.

B. Noise model and dephasing rate

As indicated in Fig. 1, the two-level system is weakly coupled to a bosonic thermal environment at temperature $T_{\rm E}$. Furthermore, we assume that the undriven qubit frequency $w_{\rm q}$ is invariant to small fluctuations in the environment; thus, the coupling to the bosonic bath is purely transverse. This yields the interaction term

$$H_{\rm SE} = \sum_k V_k(\hat{b}_k + \hat{b}_k^\dagger)\hat{\sigma}_{\rm x}, \tag{7}$$

where $\hat{b}_k$ ($\hat{b}_k^\dagger$) is the annihilation (creation) operator of an excitation in the environment and V_k gives the system-environment coupling strength.

In the case of a dc qubit ($\Omega = 0$), the environmental coupling considered here causes no pure dephasing at $b = 0$. However, the effective qubit frequency can only be modulated through the dc bias as $\mathcal{E} = \sqrt{w_{\rm q}^2 + b^2}$, where $\mathcal{E}$ is the new qubit gap under bias b. Upon applying the dc bias, the qubit gap will acquire a sensitivity to fluctuations in b as $\partial_b\mathcal{E} = b/\mathcal{E}$ [24,27,28].

The dependence of the effective qubit frequency on bias fluctuations is considerably different in Floquet qubits. Since the Floquet states are (generally) time-dependent superpositions of the static qubit eigenstates, the purely transverse coupling transforms to a combination of transverse and longitudinal coupling in the Floquet basis. The

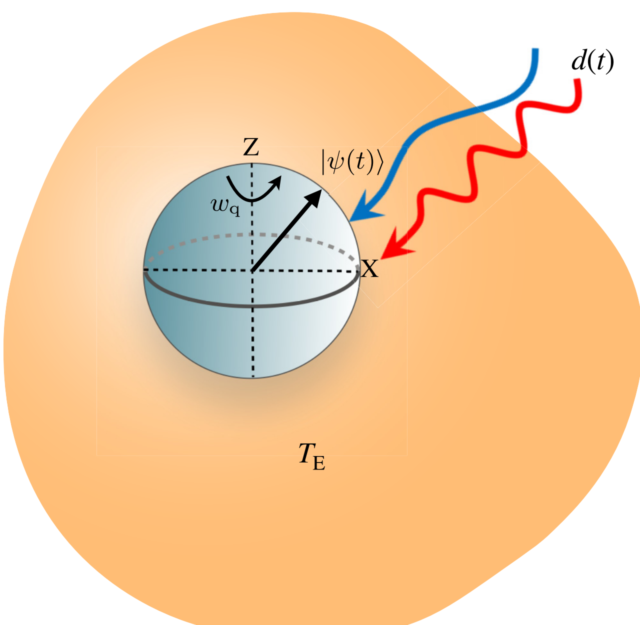

FIG. 1. Schematic depiction of a two-level system (represented by a Bloch sphere) driven by a bichromatic drive $d(t) = \Omega\cos(\nu)\cos(N_1\omega t) + \Omega\sin(\nu)\cos(N_2\omega t) + b$, where N_1 and N_2 are integers. The qubit is linearly coupled to a thermal environment at temperature $T_{\rm E}$, leading to decoherence via $1/f$ and dielectric noise channels.

instantaneous Floquet modes form an orthonormal basis for $\mathcal{H}$, so at each time t we may write

$$\hat{\sigma}_{\rm x} = g_+(t)\hat{c}_+(t) + g_+^*(t)\hat{c}_+^\dagger(t) + g_\phi(t)\hat{c}_\phi(t), \tag{8}$$

where the off-diagonal terms $\hat{c}_+(t) = |u_+(t)\rangle\langle u_-(t)|$ and $g_+(t) = {\rm Tr}\{\hat{\sigma}_{\rm x}\hat{c}_+^\dagger(t)\}$ describe the effective transverse coupling, and the diagonal terms $\hat{c}_\phi(t) = |u_+(t)\rangle\langle u_+(t)| - |u_-(t)\rangle\langle u_-(t)|$ and $g_\phi(t) = \frac{1}{2}{\rm Tr}\{\hat{\sigma}_{\rm x}\hat{c}_\phi(t)\}$ describe the effective longitudinal coupling, at time t. We are interested in the long-term evolution of the Floquet modes due to the time-dependent coupling strengths $g_\mu(t)$ and fluctuations in the environment. To simplify this analysis, it is convenient to go into an interaction picture where the evolution of the Floquet states is trivial. This can be done through the transformation unitary

$$\hat{U}_{\rm I} = \mathcal{T}\exp\left\{i\int_0^t dt'\hat{H}_{\rm S}(t')\right\} = \sum_{\sigma=\pm} e^{i\epsilon_\sigma t}|u_\sigma(0)\rangle\langle u_\sigma(t)|, \tag{9}$$

which yields

$$\tilde{\hat{\sigma}}_x(t) = \hat{U}_{\rm I}\hat{\sigma}_{\rm x}\hat{U}_{\rm I}^\dagger = g_\phi(t)\hat{c}_\phi(0) + \sum_{\mu=\pm} e^{\mu i\Delta\epsilon t}g_\mu(t)\hat{c}_\mu(0), \tag{10}$$

where we define the notation $g_-(t) = g_+^*(t)$, $\hat{c}_-(t) = \hat{c}_+^\dagger(t)$, and $\Delta\epsilon = \epsilon_+ - \epsilon_-$ is the Floquet quasienergy gap. Expanding the coupling strength matrix elements in Fourier series,

$$g_{k\pm} = \frac{\omega}{2\pi}\int_0^{2\pi/\omega} e^{-ik\omega t}{\rm Tr}\{\hat{\sigma}_{\rm x}\hat{c}_\mp(t)\}dt, \tag{11}$$

$$g_{k\phi} = \frac{\omega}{4\pi}\int_0^{2\pi/\omega} e^{-ik\omega t}{\rm Tr}\{\hat{\sigma}_{\rm x}\hat{c}_\phi(t)\}dt, \tag{12}$$

the coupling operator can be expressed as

$$\tilde{\hat{\sigma}}_x = \sum_{\substack{\mu=\pm,\phi \\ k\in\mathbb{Z}}} e^{-ik\omega_{k\mu}t}g_{k\mu}\hat{c}_\mu(0), \tag{13}$$

where $\omega_{k\pm} = k\omega \pm \Delta\epsilon$, $\omega_{k\phi} = k\omega$.

Considering weak system-environment coupling and a thermal environment, the system dynamics is given by the Floquet master equation

$$\frac{d\tilde{\hat{\rho}}_{\rm q}}{dt} = \sum_{\substack{\mu=\phi,\pm \\ k}} |g_{k\mu}|^2 S(\omega_{k\mu})\mathcal{D}[\hat{c}_\mu]\tilde{\hat{\rho}}_{\rm q}, \tag{14}$$

where $\tilde{\hat{\rho}}_{\rm q}$ is the density matrix of the two-level system in the interaction picture and $\mathcal{D}[\hat{O}]\hat{\rho}_{\rm q} = \hat{O}\hat{\rho}_{\rm q}\hat{O}^\dagger - (\hat{O}^\dagger\hat{O}\hat{\rho}_{\rm q} + \hat{\rho}_{\rm q}\hat{O}^\dagger\hat{O})/2$. The environment spectral density,

$S(\omega) = \int_{-\infty}^{\infty} dt e^{i\omega t}\mathrm{Tr}_{\mathrm{E}}[\{\tilde{\hat{b}}_k^\dagger(t) + \tilde{\hat{b}}_k(t)\}\{\tilde{\hat{b}}_k^\dagger(0) + \tilde{\hat{b}}_k(0)\}\tilde{\hat{\rho}}_{\mathrm{E}}]$, where $\tilde{\hat{b}}_k^\dagger(\tilde{\hat{b}}_k)$ is the environment annihilation (creation) operator in the interaction picture, and $\tilde{\hat{\rho}}_{\mathrm{E}}$ is the environment density matrix in the interaction picture.

Following the noise model of Ref. [24], we consider two different contributions to the environment spectral density, $S(\omega) = S_{\mathrm{f}}(\omega) + S_{\mathrm{d}}(\omega)$. The $1/f$ noise is given by $S_f(\omega) = |V_{\mathrm{f}}|^2 2\pi/|\omega|$. Additionally, the thermal noise, $S_{\mathrm{d}}(\omega) = [1 + n(\omega, T_{\mathrm{E}})]V_{\mathrm{d}}(\omega/2\pi)^2$, where $n(\omega, T_{\mathrm{E}}) = [e^{\omega/k_{\mathrm{B}}T_{\mathrm{E}}} - 1]^{-1}$, follows the Bose-Einstein distribution.

Under these considerations, the dephasing rate approximates the form [24]

$$\gamma_\phi \approx 2|V_{\mathrm{f}}|\sqrt{|\ln \omega_{\mathrm{IR}}\tau|}|g_{0\phi}| + \sum_{k\neq 0} 2|g_{k\phi}|^2 S(k\omega), \qquad (15)$$

where ω_{IR} is an infrared cutoff frequency and τ is a finite characteristic time, introduced to regularize the divergence of $1/f$ noise spectrum at $\omega = 0$ [39]. For numerical simulations, we consider system and environmental parameters appropriate for a fluxonium [24,39], a superconducting qubit design. We set $V_{\mathrm{f}} = 9.0 \times 10^{-6} w_{\mathrm{q}}$, $V_{\mathrm{d}} = 3 \times 10^{-6} w_{\mathrm{q}}$, and $\sqrt{|\ln \omega_{\mathrm{IR}}\tau|} = 4$. To emphasize thermal noise effects, most significant when the drive frequency is comparable to $k_{\mathrm{B}}T$, we set $w_{\mathrm{q}}/k_{\mathrm{B}}T = 1.43$, typical for low-frequency qubits [23,40,41].

Equation (14) suggests that the $g_{k\mu}$ weights may be interpreted as the effective time-independent transverse and longitudinal couplings to noise at frequency $k\omega$. Of particular significance is the weight $g_{0\phi}$, which quantifies the longitudinal coupling of the Floquet states to low-frequency noise. This weight enters the dephasing rate through the first term on the right-hand side of Eq. (15), which dominates the dephasing rate in the low-temperature regime. Thus, the dephasing time of a Floquet qubit is largely determined by $g_{0\phi}$, which obeys the relation [24]

$$\frac{\partial \Delta\epsilon}{\partial b} = g_{0\phi}. \qquad (16)$$

The dominating term of Eq. (15) can then be re-expressed as $|\partial_b \Delta\epsilon| V_f \sqrt{|\ln \omega_{\mathrm{IR}}\tau|}$ and may be understood as quasienergy shifts due to uncontrolled fluctuations in the parameter b (low-frequency noise). However, when $\partial_b \Delta\epsilon = 0$, the dephasing rate will be entirely determined by the quasienergy sensitivity to broadband noise [$S(k\omega)$, $k \neq 0$]. The sensitivity to ac drive amplitude noise can be particularly significant experimentally, and is related to the instrumentation noise floor and control line attenuation [42]. ac amplitude noise enters Eq. (15) through the terms $S(N_1\omega)$ and $S(N_2\omega)$, and the sensitivity $\partial_\Omega \Delta\epsilon$ through their corresponding weights $g_{N_1\phi}, g_{N_2\phi}$. In the following, we study the effect of both dc and ac noise on the dephasing time of a solid-state qubit.

II. DYNAMICAL SWEET AND SOUR MANIFOLDS

The regions where the dephasing time ($T_\phi = \gamma_\phi^{-1}$) is high are known in the literature as *dynamical sweet spots* [24,27,28,43]. Given that the dominating term in Eq. (15) is proportional to $|\partial_b \Delta\epsilon|$ (the dc noise sensitivity), T_ϕ will achieve its maximal values along the level curves in the drive parameters where $\partial_b \Delta\epsilon \approx 0$, as discussed by Huang *et al.* [24]. However, as discussed in the previous section, $|\partial_b \Delta\epsilon|$ does not uniquely determine the dephasing rate, making $\partial_b \Delta\epsilon \to 0$ a necessary but not sufficient condition for an optimal working point. Under our noise model, we find that T_ϕ at or near the dynamical sweet spots is inherently limited by the "width" of the dynamical sweet region in the parameter b. In other words, the quality of a dynamical sweet spot depends on how broad the region is where $\partial_b \Delta\epsilon \approx 0$. Moreover, in these regions of low sensitivity to dc noise, high-frequency noise becomes relevant [$S(k\omega)$, $k \neq 0$] to the coherence time. The dominant contributions to the dephasing rate will be at the fundamental drive frequencies $N_1\omega$ and $N_2\omega$ [42], which will affect T_ϕ with a distinct sensitivity to drive amplitude noise ($\partial_\Omega \Delta\epsilon$). This sensitivity should be determined by the weights $g_{N_1\phi}$ and $g_{N_2\phi}$ according to Eq. (15). We name regions with low dc noise sensitivity but high ac noise sensitivity as *dynamical sour spots*.

A. Weak-driving regime

As shown in Ref. [24], in the weak drive regime and for $b \approx 0$, we expect dynamical sweet spots near avoided crossings, which occur around $\omega \approx k w_{\mathrm{q}}$. For a monochromatic Floquet qubit, setting $k = 1$ corresponds to near-resonant driving, while $k > 1$ corresponds to off-resonant driving. Hence, for numerical simulations, we choose a bichromatic drive [Eq. (2)]

$$d(t) = \Omega[\cos\nu \cos(3w_{\mathrm{q}}t) + \sin\nu \cos(w_{\mathrm{q}}t)] + b \qquad (17)$$

with $\omega = w_{\mathrm{q}}$, $N_1 = 3$, $N_2 = 1$, $\nu \in [0, \pi/2]$, and $b/w_{\mathrm{q}} \in [-1, 1]$. In Eq. (17), $\nu = 0$ corresponds to purely off-resonant driving ($N_1 = 3$), and $\nu = \pi/2$ corresponds to near-resonant driving ($N_2 = 1$). The choice of $N_1 = 3$ for the fast drive was obtained from numerical optimization of the qubit dephasing time across different N_1 values. More generally, selecting a positive odd integer for the fast-drive frequency multiplier guarantees half-wave symmetry of the total drive. As a result, the drive Fourier spectrum contains only odd harmonics of the base frequency, which can suppress coupling to environmental noise at certain frequencies, as observed in parametrically modulated transmons [27,44]. In the following, we show that the properties of dynamical sweet spots generated by resonantly driven qubits (related to spin locking; see Refs. [10–14,24]) are markedly different from those produced by fast, off-resonant drives. Furthermore, we study

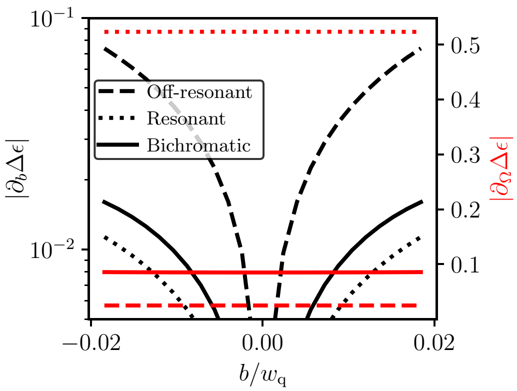

FIG. 2. On the left axis (black curves), the dc sensitivity of the quasienergy gap, $|\partial_b \Delta\epsilon|$, is plotted as a function of the dc bias b away from the static sweet spot. On the right (horizontal red lines), the sensitivity to drive amplitude noise, $|\partial_\Omega \Delta\epsilon|$, is plotted as a function of the same. Curves calculated for quasienergies generated by a drive with parameters $w = w_q$, $N_1 = 3$, $N_2 = 1$, $\Omega = 0.1 w_q$, and different mixing angles for each curve. The dashed curve corresponds to a fast drive, set by $\nu = 0$. The dotted curve corresponds to a resonant drive, set by $\nu = \pi/2$. The solid curve corresponds to a bichromatic drive, set by $\nu = \pi/30$. We calculated $|\partial_b \Delta\epsilon|$ from $g_{0\phi}$ according to Eq. (16), while $|\partial_\Omega \Delta\epsilon|$ was calculated via finite differences.

trade-offs by leveraging the distinct properties of both types of drives.

In Fig. 2, we plot $\partial_b \Delta\epsilon$ (on the left axis) as a function of the dc bias (b) on a logarithmic scale. The horizontal lines give the sensitivity to the ac noise, $\partial_\Omega \Delta\epsilon$ (on the right axis). We extract $|\partial_b \Delta\epsilon|$ from $g_{0\phi}$ following Eq. (16), while $|\partial_\Omega \Delta\epsilon|$ is evaluated by finite-difference methods. In the off-resonant case ($\nu = 0$), the sensitivity to the change in dc bias is the largest, as evidenced by higher values of $\partial_b \Delta\epsilon$ away from the narrow minimum corresponding to a dynamical sweet spot (dashed black curve). In contrast, the monochromatic resonant case ($\nu = \pi/2$) shows reduced dc sensitivity and a wider minimum (dotted black curve). However, the sensitivities are reversed for ac noise: the resonant case suffers from a large ac noise sensitivity (dotted red line) corresponding to a dynamical sour spot, whereas the off-resonant case has a lower ac noise sensitivity (dashed red line). For monochromatic drives, this sensitivity trade-off is unavoidable.

Bichromatic drives can avoid this trade-off by balancing the two sensitivities. We find that the bichromatic drive exhibits lower dc sensitivity (solid black curve) while maintaining a wider minimum and reducing ac sensitivity (solid red curve) relative to the resonant regime. As a result, a bichromatically driven Floquet qubit demonstrates improved robustness against quasienergy gap fluctuations compared to both resonant and off-resonant monochromatic drives.

The dynamical sweet and sour spots are further explored in Fig. 3, which shows (a) the dc sensitivity ($\partial_b \Delta\epsilon$), (b) the ac sensitivity ($\partial_\Omega \Delta\epsilon$), and (c) the dephasing time (T_ϕ) as functions of the dc bias (b) and the mixing angle (ν). Figure 3(a) reveals three distinct dynamical sweet spot manifolds across all mixing angles. Figure 3(b) highlights a large dynamical sour region that spans both resonant and bichromatic driving regimes, as indicated by the orange area corresponding to $\partial_\Omega \Delta\epsilon \gtrsim 10^{-1}$. The dephasing time in Fig. 3(c) has qualitative behavior closely following the dc noise sensitivity. Notably, along the dynamical sweet manifolds where $\partial_b \Delta\epsilon \to 0$, ac noise sensitivity becomes the dominant source of dephasing and sets the limit for the optimal dephasing time. As a result, T_ϕ reaches an upper bound of approximately $1.5 \times 10^7 w_q^{-1}$.

We also emphasize that the numerically implemented noise model described following Eq. (15) accounts only for $1/f$ and thermal noise. In practice, additional noise sources, particularly instrumentation noise, have been shown to significantly affect the decoherence rate of parametrically driven low-frequency qubits [40,42]. Instrumentation noise will significantly increase the deleterious

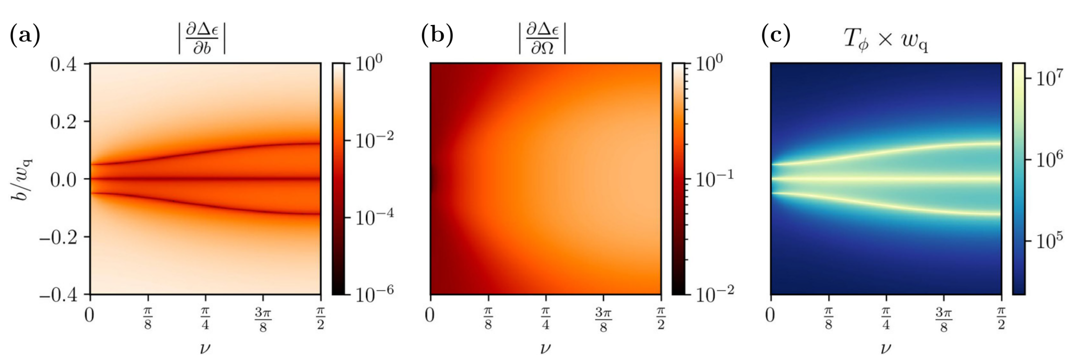

FIG. 3. Quasienergy gap sensitivities to (a) dc noise ($\partial_b \Delta\epsilon$), (b) ac noise ($\partial_\Omega \Delta\epsilon$), and (c) the resulting dephasing time (T_ϕ) plotted as functions of the mixing angle ν and the dc drive strength b, with fixed parameters $\Omega = 0.1 w_q$, $\omega = w_q$, $N_1 = 3$, $N_2 = 1$. The bichromatic case $\nu = \pi/30$ used in Fig. 2 lies within a narrow region of low ac sensitivity near $\nu \approx 0$.

effect of the dynamical sour spots shown in Fig. 3(b). This added impact of instrumentation noise falls outside the scope of this work and will be addressed in future research.

B. T_ϕ optimization beyond the weak-driving regime

In the previous section, we set $\omega = w_q$, motivated by a perturbative analysis showing that, when $\Omega \ll w_q$, the minima of $g_{0\phi}$ are expected for this choice of base frequency. In this subsection, we move beyond the weak-driving regime, taking into account the observation in Ref. [24] that, for intermediate drive strengths where fast high-fidelity gates may be implemented, the base driving frequency should be detuned from w_q to maximize T_ϕ.

We relax the weak drive assumption, and instead adopt the assumptions that neither drive is slow compared to the qubit gap ($\omega \geq w_q$) and that one drive is significantly weaker than the other (i.e., with mixing angle near 0 or $\pi/2$). With these assumptions we can derive an approximate expression for the quasienergy gap (see Appendix C for details):

$$\Delta\epsilon = \sqrt{(\omega - \Theta)^2 + (w_q \tilde{J}_{1,1}\tilde{J}_{1,2})^2}. \tag{18}$$

We define $\Theta^2 = b^2 + (w_q \tilde{J}_{0,1}\tilde{J}_{0,2})^2$, $\tilde{J}_{l,1} = J_l(\Omega\cos\nu/N_1\omega)$, and $\tilde{J}_{l,2} = J_l(\Omega\sin\nu/N_2\omega)$, where J_l is lth-order Bessel function of the first kind. We note that the above expression best predicts the quasienergy in the high-frequency regime (i.e., when $\omega \gg w_q$ or $\nu \approx 0$). Although the above expression deviates from the exact quasienergy gap for much of our numerical sweeps, it still accurately predicts the positions of the minima and maxima of the gap. We exploit this property of Eq. (18) to identify optimal frequencies that minimize $\partial_b\Delta\epsilon$. The differential of the gap with respect to the dc bias strength is given by

$$\frac{\partial\Delta\epsilon}{\partial b} = \frac{b(\omega/\Theta - 1)}{\Delta\epsilon}. \tag{19}$$

Equation (19) sets $\partial_b\Delta\epsilon = g_{0\phi}$ as directly proportional to b. Furthermore, the sensitivity to the bias vanishes when $\omega = \Theta$. That is, when

$$\omega \equiv \omega^* = \sqrt{b^2 + w_q^2 J_0^2\left(\frac{\Omega\cos\nu}{N_1\omega^*}\right)J_0^2\left(\frac{\Omega\sin\nu}{N_2\omega^*}\right)}. \tag{20}$$

When the assumptions of weak driving and small dc bias are satisfied, the above equation predicts vanishing dc noise sensitivity near $\omega \approx w_q$, consistent with the perturbative analysis and our assertion that including a resonant drive component maximally suppresses $\partial_b\Delta\epsilon$. For the intermediate drive strengths considered in this work, the optimal drive frequencies obtained from Eq. (20) are slightly detuned from the undriven qubit frequency.

In Figs. 4(a)–4(c), we analyze the dc [panel (a)] and ac [panel (b)] noise sensitivities of the quasienergy gap as functions of the dc bias strength (b) and mixing angle (ν). At each point with bias b and mixing angle ν, the drive frequency is set to a solution ω^* of Eq. (20), while $\Omega = 0.4w_q$, $N_1 = 3$, and $N_2 = 1$ are held fixed. Although the drive strength is comparable to that in Fig. 3, this new frequency-selection protocol yields a significantly richer landscape of noise-insensitive regions, highlighted by the darker areas in panels (a) and (b). ac noise sensitivity ($\partial_\Omega\Delta\epsilon$) still remains pronounced in the near-resonant, drive-dominated regime [e.g., the whiter region near $\nu \approx \pi/2$ and $b \approx 0$ in Fig. 4(b)]. However, unlike Fig. 3(b) with a nonoptimal ω, we find regions of low ac noise sensitivity even for regimes dominated by the near-resonant drive. Moreover, we identify bichromatic regions where both dc and ac noise sensitivities are simultaneously small. These *doubly sweet spots*, marked by pink dots in Fig. 4(c), correspond to enhanced dephasing times T_ϕ exceeding the maximal T_ϕ obtained in Fig. 3(c) ($1.5 \times 10^7 w_q^{-1}$). Figure 4(a) also shows an additional sweet spot manifold $\nu \approx \pi/12$ for a wide range of bias values (b), but this manifold remains sensitive to ac noise.

Figures 4(a)–4(c) show sharp variations in lifetime and noise sensitivities near the optimal operating points. This behavior arises because Eq. (20) does not admit a unique solution. In these regions, the solutions of Eq. (20) become closely clustered, and the numerical optimizer may rapidly alternate between them when selecting the optimal frequency ω^*. To mitigate these abrupt transitions, we repeated the numerical sweeps with the base frequency fixed to the optimal value determined at the high-lifetime point marked by the white star. The results of this sweep are shown in Figs. 4(d)–4(f). Compared to Figs. 3(a)–3(c), Figs. 4(d) and 4(e) show additional dc and ac sweet spot manifolds, including a doubly sweet spot manifold containing the chosen optimal base drive frequency. Even with fixed $\omega = \omega^*$, tunability along the doubly sweet spot manifold is preserved. We also note that Fig. 4(e) shows a broader region of ac insensitivity than either Fig. 4(b) or Fig. 3(b).

C. Fast-driving regime: GVV perturbation theory

In the preceding subsections, we examined the dephasing time under weak and beyond-weak driving conditions, focusing on near-resonant regimes. In this subsection, we extend our analysis to the fast-driving regime ($\omega \gg w_q$), where we explore both the quasienergy gap and the resulting dephasing time. In this regime, neither drive is resonant with the qubit gap w_q, and the strong sensitivity to ac noise observed in previous sections is negligible. Therefore, we constrain our analysis to the dc noise sensitivity $\partial_b\Delta\epsilon$. Building on our earlier results, we leverage the structure of the quasienergy gap to identify parameter regimes with

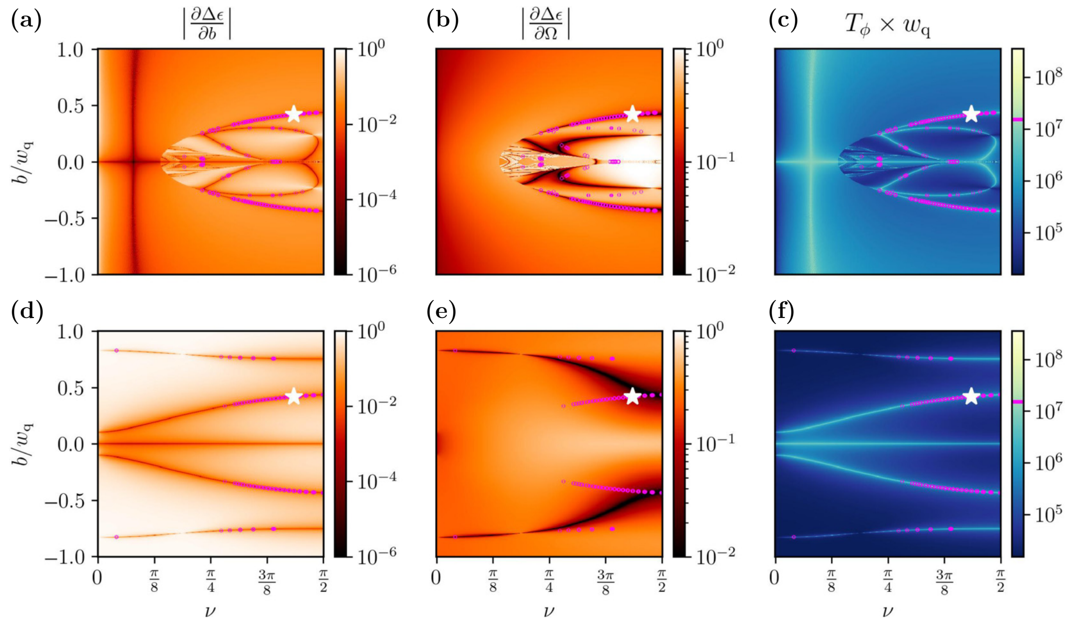

FIG. 4. Quasienergy gap sensitivities to (a),(d) dc noise ($\partial_b \Delta\epsilon$), (b),(e) ac noise ($\partial_\Omega \Delta\epsilon$), and (c),(f) the resulting dephasing time (T_ϕ) plotted as functions of the mixing angle ν and the dc drive strength b, with fixed parameters $\Omega = 0.4w_q$, $N_1 = 3$, $N_2 = 1$. For (a)–(c), the base drive frequency ω is set for each (b, ν) to a solution of Eq. (20), where the dc noise sensitivity is predicted to be minimal. For (d)–(f), the base drive frequency is fixed to a single optimal $\omega^* = 0.89w_q$ calculated for the white stars in (a)–(c). The point indicated by the white star was chosen in a doubly sweet region with low dc and ac noise sensitivities.

high dephasing time. In particular, we analyze scenarios where the Floquet states become nearly degenerate, specifically when $b \approx k\omega$ [45], where $k = mN_1 + lN_2$. We define δ through $b = k\omega + \delta$, with $0 < |\delta| \ll 1$. The rotating-wave-approximation (RWA) quasienergy gap takes the form

$$\Delta\epsilon_{\rm RWA} = \sqrt{\delta^2 + (w_q \tilde{J}_{-m,1}\tilde{J}_{-l,2})^2}, \tag{21}$$

obtained from the effective 2×2 Hamiltonian [extracted from the Floquet Hamiltonian in Eq. (C24) in Appendix C]

$$H_{\rm RWA} = \begin{pmatrix} -\dfrac{b}{2} & -\dfrac{w_q}{2}\tilde{J}_{-m,1}\tilde{J}_{-l,2} \\ -\dfrac{w_q}{2}\tilde{J}_{-m,1}\tilde{J}_{-l,2} & \dfrac{b}{2} - mN_1\omega - lN_2\omega \end{pmatrix}, \tag{22}$$

obtained in the RWA, with $\tilde{J}_{l,1}$ and $\tilde{J}_{l,2}$ as defined below Eq. (18).

To calculate the ac Stark shift correction (χ) to the RWA quasienergy gap, we apply the GVV nearly degenerate perturbation theory [45], accounting for the influence of levels beyond those selected by the degeneracy condition. We employ the GVV method, considering higher-order perturbations in w_q/ω, in contrast to the RWA, where only the zeroth-order perturbative effect is considered. The effective 2×2 GVV Hamiltonian includes the ac Stark shift χ:

$$H_{\rm GVV} = \begin{pmatrix} -\dfrac{b}{2} + \chi & -\dfrac{w_q}{2}\tilde{J}_{-m,1}\tilde{J}_{-l,2} \\ -\dfrac{w_q}{2}\tilde{J}_{-m,1}\tilde{J}_{-l,2} & \dfrac{b}{2} - mN_1\omega - lN_2\omega - \chi \end{pmatrix} \tag{23}$$

with the quasienergy gap given by the relation

$$\Delta\epsilon_{\rm GVV} = \sqrt{\Delta\epsilon_{\rm RWA}^2 + 4\chi\delta + 4\chi^2}. \tag{24}$$

Using the GVV method, we obtain the following expression for the ac Stark shift up to the leading order (see Appendix C 1):

$$\chi = \sum_{\substack{j,p=-\infty \\ j,p\neq -m,-l}}^{\infty} \frac{-(\tilde{J}_{j,1}\tilde{J}_{p,2})^2}{4(b + jN_1\omega + pN_2\omega)} w_q^2 + \mathcal{O}\left(\frac{w_q}{\omega}\right)^3. \tag{25}$$

Using Eq. (24), the dc bias sensitivity is given by

$$\frac{\partial \Delta\epsilon_{\rm GVV}}{\partial b} = \frac{1}{\Delta\epsilon_{\rm GVV}}(\delta + 2\chi)\left(1 + 2\frac{\partial \chi}{\partial b}\right). \tag{26}$$

We find that in the fast-driving regime ($\omega/w_q \gg 1$), $\partial_b\chi \ll 1$. Hence, Eq. (26) reduces to

$$\frac{\partial\Delta\epsilon_{\mathrm{GVV}}}{\partial b} \approx \frac{1}{\Delta\epsilon_{\mathrm{GVV}}}(\delta + 2\chi). \tag{27}$$

Figure 5(a) shows the dependence of the quasienergy gap on one of the drive amplitudes $\Omega_1 \equiv \Omega\cos\nu$, keeping the other drive amplitude fixed and weak compared to ω, $\Omega_2 \equiv \Omega\sin\nu = 0.1\omega$. We compare the quasienergy gaps obtained from the RWA (solid horizontal purple line) and the GVV (dashed blue curve) Hamiltonians to the exact values calculated numerically (solid red curve). The GVV result, which incorporates the ac Stark shift χ, shows markedly better agreement with numerical simulations than the RWA, with disagreement when $\Omega_1 \le \omega$.

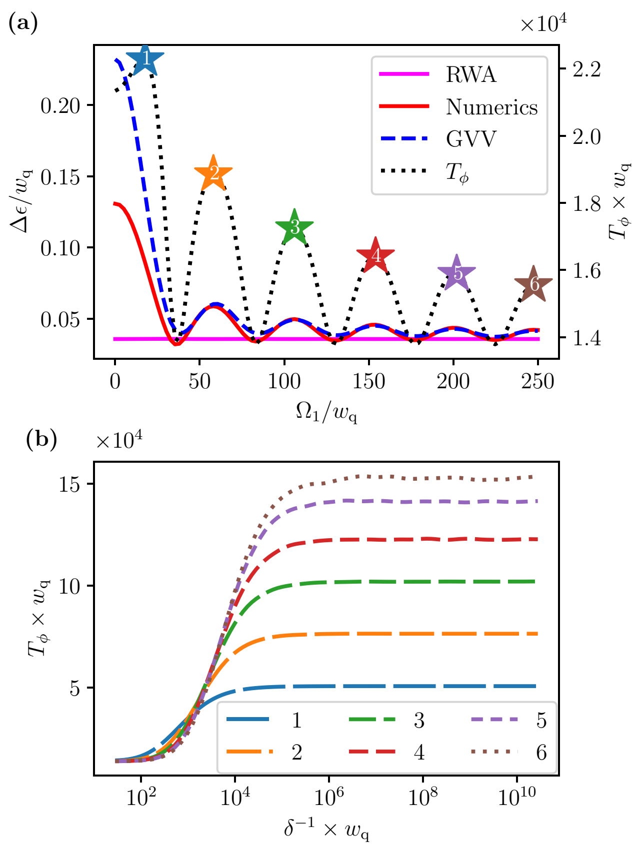

FIG. 5. (a) On the left axis, the Floquet quasienergy gap, plotted as a function $\Omega_1 = \Omega\cos(\nu)$ with $\Omega_2 = \Omega\sin(\nu)$, is held constant. We compare the exact numerical results (solid red line) with the RWA (solid purple) and GVV (dashed blue) calculations. On the right axis, the dephasing time for the same system is shown. Numbered stars correspond to local maxima of T_ϕ. (b) The dephasing time T_ϕ plotted as a function of δ at each local maximum indicated in (a). Parameters: $N_1 = 3$, $N_2 = 1$, $m = 1$, $l = -2$, $\Omega_2 = w_q$, and $\omega = 10w_q$. The bias b is set by the nearly degenerate condition and δ. In (a) $\delta = 0.01w_q$.

For fixed $\delta > 0$, the dc noise sensitivity is primarily determined by the magnitude of the quasienergy gap and the ac Stark shift χ [see Eq. (27)]; a larger quasienergy gap or ac Stark shift (since $\chi < 0$) leads to lower noise sensitivity. The ac Stark shift follows the minima and maxima of the quasienergy gap. Consequently, the dephasing time (dotted black curve) reaches its minima and maxima (indicated by stars) at the corresponding minima and maxima of the quasienergy gap, respectively.

To further analyze these maxima, in Fig. 5(b), we plot the dephasing times, using colors corresponding to each star in Fig. 5(a), as a function of δ^{-1}. We note from Eq. (27) that the dc noise sensitivity can be minimized by making δ comparable to 2χ. For large δ (small δ^{-1}), the aforementioned compensation results in a monotonous increase of the dephasing time as a function of δ^{-1}. However, as $\delta \to 0$ (large δ^{-1}), the dephasing time saturates as both the quasienergy gap and the ac Stark shift become independent of δ and take a constant value.

III. CONCLUSION AND OUTLOOK

Our work establishes bichromatic driving as a powerful strategy to engineer dynamical sweet manifolds in solid-state driven qubits, achieving high dephasing time while maintaining tunability. By combining near-resonant and off-resonant drives, we suppress sensitivity to low-frequency (e.g., $1/f$) noise by redirecting the dominant sources of decoherence to frequency regions where environmental noise is minimal. Crucially, we identify not only high-coherence “sweet spots” but also “sour spots,” where the quasienergy gap is especially sensitive to noise at the drive frequency. These sour spots become prominent when one of the drives is nearly resonant with the qubit’s dc gap; however, introducing a nearly resonant drive can also broaden the dynamical sweet region. Hence, the interplay of sweet- and sour-spot dynamics provides a framework to balance tunability and dephasing time, which is critical for single- and multiqubit operations.

Central to our work is the derivation of analytic expressions for the sensitivity of the Floquet quasienergy gap to external drives in the intermediate-strength- and fast-driving regimes. We employed the derived analytic expressions to connect the drive parameters to the dephasing time, explaining the emergence of dynamical sweet and sour spots. The analytic expressions were further employed to find optimal drive frequencies, giving a long dephasing time.

Future work will investigate the application of bichromatic Floquet engineering for single- and multiqubit gate operations. We would also like to study the application of Floquet engineering in multiqubit architectures, suppressing crosstalk while preserving tunable interactions. It would also be important to investigate how instrumentation noise affects the structure and effectiveness of the dynamical sweet and sour manifolds in low-frequency qubits. Experimental validation of our results in circuit QED platforms will bridge theory and device-specific noise landscapes to advance decoherence mitigation in parametrically driven solid-state quantum architectures.

ACKNOWLEDGMENTS

We thank Abhishek Chakraborty, Nicolas Didier, Jens Koch, and Rosario Fazio for valuable discussions. This work was supported by the U.S. Army Research Office under Grant W911NF-22-1-0258. D.D. acknowledges support from PNRR MUR Project No. PE0000023-NQSTI (National Quantum Science and Technology Institute). Y.K. is supported by the National Research Foundation of Korea (NRF) grant, funded by the Korean government (MSIT; Grants No. RS-2024-00353348 and No. RS-2023-NR068116).

DATA AVAILABILITY

The data that support the findings of this article are not publicly available. The data are available from the authors upon reasonable request.

APPENDIX A: QUANTUM FLOQUET THEORY

We consider a time-dependent, periodic Hamiltonian with period T. The corresponding Schrödinger equation (setting $\hbar = 1$),

$$i\frac{\partial}{\partial t}|\psi\rangle = \hat{H}(t)|\psi\rangle, \tag{A1}$$

does not admit any stationary eigenstates. It does, however, admit orthonormal, quasistationary solutions called Floquet states,

$$|\psi_\pm(t)\rangle = e^{-i\epsilon_\pm t}|u_\pm(t)\rangle, \tag{A2}$$

where $\epsilon_\pm$ are quasienergies, and $|u_\pm(t)\rangle$ are T-periodic Floquet modes. Note that the quasienergies are defined only up to additive factors of $\omega = 2\pi/T$, such that $\epsilon_\pm \equiv \epsilon_\pm + k\omega$ for any integer k. The quasienergies and their respective Floquet modes are eigenvalues and eigenvectors of a Hermitian operator called the Floquet Hamiltonian:

$$\hat{H}_\mathrm{F}(t) = \hat{H}(t) - i\frac{\partial}{\partial t}. \tag{A3}$$

The problem of finding the time-dependent dynamics may thus be recast as an eigenvalue problem for a time-dependent operator. We may further reduce the problem to a time-independent eigenvalue problem by exploiting the periodicity of the Floquet modes. The modes may be expanded as

$$|u_\pm\rangle = \sum_{n,\alpha} c^\pm_{n,\alpha} e^{in\omega t}|\alpha\rangle, \tag{A4}$$

where $c^\alpha_{n,\pm} = (1/T)\int_0^T e^{-in\omega t}\langle\alpha|u_\pm\rangle dt$ are the time-independent Floquet coefficients. The set of products $e^{in\omega t}|\alpha\rangle$ satisfies the properties of a product space $\mathcal{T}\otimes\mathcal{H}$ between the space of T-periodic functions $\mathcal{T}$ and atomic states of the undriven system $\mathcal{H}$. Setting the basis for $\mathcal{T}$ as $\{|n\rangle = e^{in\omega t}\}_{n\in\mathbb{Z}}$, we may write the Floquet modes as

$$|u_\pm\rangle = \sum_{n,\alpha} c^\pm_{n,\alpha}|n,\alpha\rangle. \tag{A5}$$

For notational clarity, we use Greek indices to represent the Floquet modes or atomic states, while Latin indices are used for T-periodic functions. When written in these coordinates, called the extended Hilbert space, the Floquet Hamiltonian takes the form of an infinite-dimensional time-independent operator with components $\langle n,\alpha|\hat{H}_\mathrm{F}|m,\beta\rangle$, eigenvalues $\epsilon^k_\pm$, and eigenvectors $|u^k_\pm\rangle$. The extended Hilbert space eigenvalue-vector pairs correspond to the quasienergies and modes in Eq. (A2) shifted in energy and frequency by $k\omega$:

$$\epsilon^k_\pm = \epsilon_\pm - k\omega, \tag{A6}$$

$$|u^k_\pm\rangle = \sum_{n,\alpha} c^\pm_{n,\alpha}|n-1,\alpha\rangle. \tag{A7}$$

The physically observable modes and quasienergies correspond to the equivalence classes over every k of these eigenvalues and eigenvectors. When we require a numerical result, we pick $k = 0$, but we remark that all physically measurable quantities we report are invariant to the choice of k.

In this appendix, we utilized Shirley's Floquet theory [46] to define the Floquet quasienergies and modes, a framework well suited for computational analysis due to its ability to directly extend the monochromatic framework to bichromatic driving without introducing significant complexity. However, for deriving the analytic expressions governing the quasienergy gap (see Appendix C) and for probing the multiphoton resonance regime (see Appendix C 1), we adopt multimode Floquet theory [47], which is more suited for analytic calculations.

APPENDIX B: FLOQUET HAMILTONIAN

In this appendix, we calculate the right-hand side of Eq. (3) using Hamiltonian (8) from the main text. We choose our basis $|m,\alpha\rangle = e^{im\omega t}|\alpha\rangle$, and define $\langle k,\beta|$ as the linear functional that acts on $|m,\alpha\rangle$ such that

$$\langle k,\beta|m,\alpha\rangle = \langle\beta|\alpha\rangle \int_0^T dt\, e^{-ik\omega t} e^{im\omega t}. \tag{B1}$$

The action of $-i\partial_t$ on $|m,\alpha\rangle$ and $\hat{H}(t)$ is given, respectively, by

$$-i\frac{\partial}{\partial t} e^{im\omega t}|\alpha\rangle = m\omega e^{im\omega t}|\alpha\rangle = m\omega |m,\alpha\rangle \tag{B2}$$

and

$$\hat{H}(t)|m,\alpha\rangle = -\frac{w_q}{2} e^{im\omega t}\hat{\sigma}_{\mathrm{z}}|\alpha\rangle + \frac{d(t)}{2} e^{imwt}\hat{\sigma}_{\mathrm{x}}|\alpha\rangle . \tag{B3}$$

Considering the drive to be combinations of complex exponentials,

$$d(t) = \frac{\Omega}{2}[\cos\nu(e^{iN_1\omega t} + e^{-iN_1\omega t}) + \sin\nu(e^{iN_2\omega t} + e^{-iN_2\omega t})] + b, \tag{B4}$$

we obtain

$$\begin{aligned} d(t)e^{imwt} &= \frac{\Omega}{2}[\cos\nu(e^{i(m+N_1)\omega t} + e^{i(m-N_1)\omega t}) + \sin\nu(e^{i(m+N_2)\omega t} + e^{i(m-N_2)\omega t})] + e^{im\omega t}b \\ &= \frac{\Omega}{2}[\cos\nu\big(|m+N_1\rangle + |m-N_1\rangle\big) + \sin\nu\big(|m+N_2\rangle + |m-N_2\rangle\big)] + b\,|m\rangle . \end{aligned} \tag{B5}$$

Thus, the action of the time-dependent Hamiltonian on a basis state is given by

$$\begin{aligned} \hat{H}(t)|m,\alpha\rangle = &-\frac{w_q}{2}|m\rangle\otimes\hat{\sigma}_z|\alpha\rangle + \frac{b}{2}|m\rangle\otimes\hat{\sigma}_x|\alpha\rangle \\ &+ \frac{\Omega}{4}[\cos\nu(|m+N_1\rangle + |m-N_1\rangle) + \sin\nu(|m+N_2\rangle + |m-N_2\rangle)]\otimes\hat{\sigma}_x|\alpha\rangle . \end{aligned} \tag{B6}$$

Note that the time dependence of the Hamiltonian has been incorporated into the basis vectors, leaving all coefficients time independent. Hence, the Floquet Hamiltonian in the $|m,\alpha\rangle$ basis can be expressed as

$$\begin{aligned} \hat{H}(t) - i\frac{\partial}{\partial t} = \sum_m |m\rangle\langle m| \otimes \left(-\frac{w_q}{2}\hat{\sigma}_{\mathrm{z}} + \frac{b}{2}\hat{\sigma}_{\mathrm{x}} + m\omega\right) + \frac{\Omega}{4}[\cos\nu(|m+N_1\rangle\langle m| + |m-N_1\rangle\langle m|) \\ + \sin\nu(|m+N_2\rangle\langle m| + |m-N_2\rangle\langle m|)]\otimes\hat{\sigma}_{\mathrm{x}}. \end{aligned} \tag{B7}$$

The Floquet Hamiltonian in Eq. (B7) separates into the terms $\hat{H}_0, \hat{H}_{\mathrm{dc}}, \hat{H}_{\mathrm{ac}}$ defined in Eqs. (4)–(6), respectively. The Hamiltonian $\hat{H}_0 + \hat{H}_{\mathrm{dc}}$ is easily diagonalized with eigenvalues ($\lambda_\pm^m$) and eigenvectors ($|m,\pm\rangle$), where

$$\lambda_\pm^m = m\omega \pm \tfrac{1}{2}\mathcal{E}, \tag{B8}$$

$$|m,+\rangle = \cos\theta\,|m,g\rangle + \sin\theta\,|m,e\rangle , \tag{B9}$$

$$|m,-\rangle = \sin\theta\,|m,g\rangle - \cos\theta\,|m,e\rangle . \tag{B10}$$

Here, g, e enumerate the $\hat{\sigma}_{\mathrm{x}}$ eigenstates, $\theta = \frac{1}{2}\tan^{-1}(b/w_{\mathrm{q}})$, and $\mathcal{E} = \sqrt{w_{\mathrm{q}}^2 + b^2}$ is the transition frequency of the undriven qubit. In this new basis, the $\hat{H}_0 + \hat{H}_{\mathrm{dc}}$, $\hat{\sigma}_{\mathrm{x}}$, and $\hat{\sigma}_{\mathrm{z}}$ operators reduce to

$$\begin{gathered} \hat{H}_0 + \hat{H}_{\mathrm{dc}} = \sum_m |m\rangle\langle m| \otimes \big[m\omega + \tfrac{1}{2}\mathcal{E}\big(|+\rangle\langle +| - |-\rangle\langle -|\big)\big], \\ \hat{\sigma}_{\mathrm{z}} = \begin{bmatrix} \cos 2\theta & \sin 2\theta \\ \sin 2\theta & -\cos 2\theta \end{bmatrix}, \quad \text{and} \quad \hat{\sigma}_{\mathrm{x}} = \begin{bmatrix} \sin 2\theta & -\cos 2\theta \\ -\cos 2\theta & -\sin 2\theta \end{bmatrix}. \end{gathered} \tag{B11}$$

APPENDIX C: QUASIENERGY GAP

In this appendix, we use multimode Floquet theory to calculate an analytic expression for the quasienergy gap. Multimode Floquet theory exploits the presence of two periodic drives of commensurate frequencies to expand the Floquet modes in terms of two periodic functions as

$$|u_\sigma(t)\rangle = \sum_{\substack{m,l\\ \alpha=\pm}} c_{ml}^{\sigma,\alpha} \left|u_\alpha^{ml}\right\rangle, \tag{C1}$$

where $\sigma = \{+,-\}$ and $\left|u_\alpha^{ml}\right\rangle = e^{imN_1\omega t}e^{ilN_2\omega t}\,|\alpha\rangle$. Unlike in Shirley's formulation of Floquet theory, in multimode Floquet theory we treat the product $e^{imN_1\omega t}e^{ilN_2\omega t}$ as a vector in a product space $\mathcal{T}_1 \otimes \mathcal{T}_2$ of periodic functions with periods $2\pi/N_1\omega$ and $2\pi/N_2\omega$, respectively. This defines

$$|m,l\rangle = e^{imN_1\omega t}e^{ilN_2\omega t} = |m\rangle \otimes |l\rangle\,, \tag{C2}$$

and thus $\left|u_\alpha^{ml}\right\rangle = |m\rangle \otimes |l\rangle \otimes |\alpha\rangle$ is a triple Kronecker product. Following Ref. [45], we rotate the Hamiltonian $\hat{H}(t) = -w_{\mathrm{q}}/2\hat{\sigma}_{\mathrm{z}} + d(t)/2\hat{\sigma}_{\mathrm{x}}$ by a $\pi/2$ rotation around the y axis, such that

$$H_{\mathrm{q}} = -\frac{w_{\mathrm{q}}}{2}\hat{\sigma}_{\mathrm{x}} - \frac{d(t)}{2}\hat{\sigma}_{\mathrm{z}}. \tag{C3}$$

Using multimode Floquet theory, the eigenequation for the Floquet Hamiltonian can be written as

$$\begin{aligned}&\left(-\frac{w_{\mathrm{q}}}{2}\hat{\sigma}_{\mathrm{x}} - \frac{b}{2}\hat{\sigma}_{\mathrm{z}} + mN_1\omega + lN_2\omega\right)\left|u_\sigma^{ml}\right\rangle - \frac{\Omega}{4}\cos\nu\hat{\sigma}_{\mathrm{z}}(|u_\sigma^{(m-1)l}\rangle + |u_\sigma^{(m+1)l}\rangle)\\ &-\frac{\Omega}{4}\sin\nu\hat{\sigma}_{\mathrm{z}}(|u_\sigma^{m(l-1)}\rangle + |u_\sigma^{m(l+1)}\rangle) = \epsilon_\sigma|u_\sigma^{ml}\rangle.\end{aligned} \tag{C4}$$

Hence, the Floquet Hamiltonian matrix in the basis $\mathcal{T}_1 \otimes \mathcal{T}_2$ would be given by

$$\hat{H}_{\mathrm{F}} = \begin{bmatrix} \ddots & & & & & & & & & & & & \\ & M_{-1,-1} & R & 0 & \cdots & D & 0 & 0 & \cdots & 0 & 0 & 0 & \\ & R & M_{-1,0} & R & \cdots & 0 & D & 0 & \cdots & 0 & 0 & 0 & \\ & 0 & R & M_{-1,+1} & \cdots & 0 & 0 & D & \cdots & 0 & 0 & 0 & \\ & \vdots & \vdots & \vdots & \ddots & \vdots & \vdots & \vdots & \ddots & \vdots & \vdots & \vdots & \\ & D & 0 & 0 & \cdots & M_{0,-1} & R & 0 & \cdots & D & 0 & 0 & \\ & 0 & D & 0 & \cdots & R & M_{0,0} & R & \cdots & 0 & D & 0 & \\ & 0 & 0 & D & \cdots & 0 & R & M_{0,+1} & \cdots & 0 & 0 & D & \\ & \vdots & \vdots & \vdots & \ddots & \vdots & \vdots & \vdots & \ddots & \vdots & \vdots & \vdots & \\ & 0 & 0 & 0 & \cdots & D & 0 & 0 & \cdots & M_{+1,-1} & R & 0 & \\ & 0 & 0 & 0 & \cdots & 0 & D & 0 & \cdots & R & M_{+1,0} & R & \\ & 0 & 0 & 0 & \cdots & 0 & 0 & D & \cdots & 0 & R & M_{+1,+1} & \\ & & & & & & & & & & & & \ddots \end{bmatrix}, \tag{C5}$$

where

$$M_{ml} = \begin{bmatrix} -\frac{b}{2} + mN_1\omega + lN_2\omega & -\frac{w_{\mathrm{q}}}{2} \\ -\frac{w_{\mathrm{q}}}{2} & \frac{b}{2} + mN_1\omega + lN_2\omega \end{bmatrix} \tag{C6}$$

and

$$D = \begin{bmatrix} -\frac{\Omega}{4}\cos\nu & 0 \\ 0 & \frac{\Omega}{4}\cos\nu \end{bmatrix}, \qquad R = \begin{bmatrix} -\frac{\Omega}{4}\sin\nu & 0 \\ 0 & \frac{\Omega}{4}\sin\nu \end{bmatrix}. \tag{C7}$$

Taking the energy gap $-w_\mathrm{q}$ as the perturbation parameter, we divide the Floquet matrix into two parts: an unperturbed part $H_{0,\mathrm{F}}$ and a perturbed part $(-w_\mathrm{q}/2)V'$,

$$H_\mathrm{F} = H_{0,\mathrm{F}} + \frac{(-w_\mathrm{q})}{2}V'. \tag{C8}$$

The unperturbed part of the Floquet matrix can thus be written as

$$H_{0,\mathrm{F}} = \begin{bmatrix} \ddots & & & & & & & & & & & & \\ & -\frac{b}{2}-N_\Sigma\omega & 0 & -\frac{\Omega}{4}\sin\nu & 0 & 0 & 0 & \cdots & -\frac{\Omega}{4}\cos\nu & 0 & 0 & 0 & \\ & 0 & \frac{b}{2}-N_\Sigma\omega & 0 & \frac{\Omega}{4}\sin\nu & 0 & 0 & \cdots & 0 & \frac{\Omega}{4}\cos\nu & 0 & 0 & \\ & -\frac{\Omega}{4}\sin\nu & 0 & -\frac{b}{2}-N_1\omega & 0 & -\frac{\Omega}{4}\sin\nu & 0 & \cdots & 0 & 0 & -\frac{\Omega}{4}\cos\nu & 0 & \\ & 0 & \frac{\Omega}{4}\sin\nu & 0 & \frac{b}{2}-N_1\omega & 0 & \frac{\Omega}{4}\sin\nu & \cdots & 0 & 0 & 0 & \frac{\Omega}{4}\cos\nu & \\ & 0 & 0 & -\frac{\Omega}{4}\sin\nu & 0 & -\frac{b}{2}-N_\Delta\omega & 0 & \cdots & 0 & 0 & 0 & 0 & \\ & 0 & 0 & 0 & \frac{\Omega}{4}\sin\nu & 0 & \frac{b}{2}-N_\Delta\omega & \cdots & 0 & 0 & 0 & 0 & \\ & \vdots & \vdots & \vdots & \ddots & \vdots & \vdots & \vdots & \ddots & \vdots & \vdots & \vdots & \\ & -\frac{\Omega}{4}\cos\nu & 0 & 0 & 0 & 0 & 0 & \cdots & -\frac{b}{2}-N_2\omega & 0 & -\frac{\Omega}{4}\sin\nu & 0 & \\ & 0 & \frac{\Omega}{4}\cos\nu & 0 & 0 & 0 & 0 & \cdots & 0 & \frac{b}{2}-N_2\omega & 0 & \frac{\Omega}{4}\sin\nu & \\ & 0 & 0 & -\frac{\Omega}{4}\cos\nu & 0 & 0 & 0 & \cdots & -\frac{\Omega}{4}\sin\nu & 0 & -\frac{b}{2} & 0 & \\ & 0 & 0 & 0 & \frac{\Omega}{4}\cos\nu & 0 & 0 & \cdots & 0 & \frac{\Omega}{4}\sin\nu & 0 & \frac{b}{2} & \\ & & & & & & & & & & & & \ddots \end{bmatrix}, \tag{C9}$$

where $N_{\Sigma/\Delta} = N_1 \pm N_2$. The perturbed part, on the other hand, is given by

$$V' = \begin{bmatrix} \ddots & & & & & & & & & & & & \\ & 0 & 1 & 0 & 0 & 0 & 0 & \cdots & 0 & 0 & 0 & 0 & \\ & 1 & 0 & 0 & 0 & 0 & 0 & \cdots & 0 & 0 & 0 & 0 & \\ & 0 & 0 & 0 & 1 & 0 & 0 & \cdots & 0 & 0 & 0 & 0 & \\ & 0 & 0 & 1 & 0 & 0 & 0 & \cdots & 0 & 0 & 0 & 0 & \\ & 0 & 0 & 0 & 0 & 0 & 1 & \cdots & 0 & 0 & 0 & 0 & \\ & 0 & 0 & 0 & 0 & 1 & 0 & \cdots & 0 & 0 & 0 & 0 & \\ & \vdots & \vdots & \vdots & \ddots & \vdots & \vdots & \vdots & \ddots & \vdots & \vdots & \vdots & \\ & 0 & 0 & 0 & 0 & 0 & 0 & \cdots & 0 & 1 & 0 & 0 & \\ & 0 & 0 & 0 & 0 & 0 & 0 & \cdots & 1 & 0 & 0 & 0 & \\ & 0 & 0 & 0 & 0 & 0 & 0 & \cdots & 0 & 0 & 0 & 1 & \\ & 0 & 0 & 0 & 0 & 0 & 0 & \cdots & 0 & 0 & 1 & 0 & \\ & & & & & & & & & & & & \ddots \end{bmatrix}. \tag{C10}$$

The eigenvalues and eigenvectors of matrix $H_{0,\mathrm{F}}$ can be solved in terms of Bessel functions $J_k(\mp\Omega\cos\nu/2N_1\omega)$ and $J_k(\mp\Omega\sin\nu/2N_2\omega)$ [45,48]. The appropriate transformation of the basis can be obtained by considering the eigenvalue problem

$$\left(\mathcal{H}(t) - i\frac{\partial}{\partial t}\right)\phi(t) = \lambda\phi(t), \tag{C11}$$

where $\mathcal{H}(t) = -b/2 + (\Omega/2)\cos\nu\cos N_1\omega t + (\Omega/2)\sin\nu\cos N_2\omega t$. The eigenvector for the trivial solution $\lambda = -b/2$ would be

$$\phi(t) = \exp\left[-i\left(\frac{\Omega\cos\nu}{2N_1\omega}\sin N_1\omega t + \frac{\Omega\sin\nu}{2N_2\omega}\sin N_2\omega t\right)\right] = \sum_{k_1,k_2=-\infty}^{+\infty} J_{k_1}\left(-\frac{\Omega\cos\nu}{2N_1\omega}\right)J_{k_2}\left(-\frac{\Omega\sin\nu}{2N_2\omega}\right)e^{i(k_1N_1+k_2N_2)\omega t}. \tag{C12}$$

Similarly, for the choice of $\mathcal{H}(t) = b/2 + (\Omega/2)\cos\nu\cos N_1\omega t + (\Omega/2)\sin\nu\cos N_2\omega t$ and $\lambda = b/2$, we have the solution

$$\phi(t) = \exp\left[i\left(\frac{\Omega\cos\nu}{2N_1\omega}\sin N_1\omega t + \frac{\Omega\sin\nu}{2N_2\omega}\sin N_2\omega t\right)\right] = \sum_{k_1=-\infty}^{+\infty}\sum_{k_2=-\infty}^{+\infty} J_{k_1}\left(\frac{\Omega\cos\nu}{2N_1\omega}\right)J_{k_2}\left(\frac{\Omega\sin\nu}{2N_2\omega}\right)e^{i(k_1N_1+k_2N_2)\omega t}. \tag{C13}$$

Now the eigenvectors for the solutions $\lambda = \mp b/2 + mN_1\omega + lN_2\omega$ are given by

$$\phi^{ml}(t) = \sum_{k_1=-\infty}^{+\infty}\sum_{k_2=-\infty}^{+\infty} J_{k_1-m}\left(\mp\frac{\Omega\cos\nu}{2N_1\omega}\right)J_{k_2-l}\left(\mp\frac{\Omega\sin\nu}{2N_2\omega}\right)e^{i(k_1N_1+k_2N_2)\omega t}. \tag{C14}$$

To make our analysis of the Floquet matrix H_{F} convenient, we can enforce a change of basis of $H_{0,\mathrm{F}}$. The new basis in which $H_{0,\mathrm{F}}$ is diagonal is related to the existing one as

$$\left|\phi_{\pm}^{ml}\right\rangle = \sum_{k_1=-\infty}^{+\infty}\sum_{k_2=-\infty}^{+\infty} J_{k_1-m}\left(\mp\frac{\Omega\cos\nu}{2N_1\omega}\right)J_{k_1-l}\left(\mp\frac{\Omega\sin\nu}{2N_2\omega}\right)|u_{\pm}^{k_1k_2}\rangle. \tag{C15}$$

The next step is to write the Floquet matrix H_{F} in the changed basis. We can do this because the difference between H_{F} and $H_{0,\mathrm{F}}$ is just a perturbative term. First, we calculate the off-diagonal elements of this new matrix. We start this exercise by making the observation that

$$\left\langle u_{\pm}^{ml}\right| H_{\mathrm{F}}|u_{\mp}^{jk}\rangle = -\frac{w_{\mathrm{q}}}{2}\delta_{mj}\,\delta_{lk}. \tag{C16}$$

Using Eqs. (C15) and (C16), and the identities

$$J_k(-x) = J_{-k}(x) \quad \text{and} \quad \sum_{k=-\infty}^{+\infty} J_{n+k}(x)J_{n-k}(x) = J_n(2x), \tag{C17}$$

we obtain

$$\left\langle \phi_{\mp}^{ml}\right| H_F|\phi_{\pm}^{jk}\rangle = -\frac{w_{\mathrm{q}}}{2}J_{\pm(j-m)}\left(\frac{\Omega\cos\nu}{N_1\omega}\right)J_{\pm(k-l)}\left(\frac{\Omega\sin\nu}{N_2\omega}\right). \tag{C18}$$

Similarly, the diagonal entries of the new matrix can be obtained by using the fact

$$\left\langle u_{\pm}^{ml}\right| H_F|u_{\pm}^{jk}\rangle = \left(\mp\frac{b}{2} + mN_1\omega + lN_2\omega\right)\delta_{mj}\,\delta_{lk} \mp \frac{\Omega}{4}\sin\nu(\delta_{mj}\,\delta_{l,k+1} + \delta_{mj}\,\delta_{l,k-1}) \mp \frac{\Omega}{4}\cos\nu(\delta_{m,j+1}\delta_{lk} + \delta_{m,j-1}\delta_{lk}) \tag{C19}$$

and the identities

$$J_{k-1}(x) + J_{k+1}(x) = \frac{2k}{x}J_k(x),$$
$$\sum_k J_k(x) + J_{k-n}(x) = \sum_k J_k(x) + J_{n-k}(-x) = J_n(0) = \delta_{n0}. \tag{C20}$$

Therefore,

$$\langle\phi_{\pm}^{ml}|\,H_F|\phi_{\pm}^{jk}\rangle = \left(\mp\frac{b}{2} + mN_1\omega + lN_2\omega\right)\delta_{mj}\,\delta_{lk}. \tag{C21}$$

Equations (C18) and (C21) jointly give the Floquet matrix in the new basis.

We define

$$D_{m,l}^{0,0} = \begin{bmatrix} \langle\phi_{+}^{ml}|\,H_F\,|\phi_{+}^{ml}\rangle & \langle\phi_{+}^{ml}|\,H_F\,|\phi_{-}^{ml}\rangle \\ \langle\phi_{-}^{ml}|\,H_F\,|\phi_{+}^{ml}\rangle & \langle\phi_{-}^{ml}|\,H_F\,|\phi_{-}^{ml}\rangle \end{bmatrix} = \begin{bmatrix} -\frac{b}{2} + mN_1\omega + lN_2\omega & -\frac{w_{\mathrm{q}}}{2}J_0\left(\frac{\Omega\cos\nu}{N_1\omega}\right)J_0\left(\frac{\Omega\sin\nu}{N_2\omega}\right) \\ -\frac{w_{\mathrm{q}}}{2}J_0\left(\frac{\Omega\cos\nu}{N_1\omega}\right)J_0\left(\frac{\Omega\sin\nu}{N_2\omega}\right) & \frac{b}{2} + mN_1\omega + lN_2\omega \end{bmatrix}, \tag{C22}$$

and, for $\kappa_l, \kappa_m \neq 0$,

$$D_{m,l}^{\kappa_m,\kappa_l} = \begin{bmatrix} 0 & \langle\phi_{+}^{ml}|\,H_F|\phi_{-}^{m+\kappa_m\; l+\kappa_l}\rangle \\ \langle\phi_{-}^{ml}|\,H_F|\phi_{+}^{m+\kappa_m\; l+\kappa_l}\rangle & 0 \end{bmatrix}. \tag{C23}$$

In the new basis, the Floquet Hamiltonian H_{F} can be rewritten as

$$\tilde{H}_F = \begin{bmatrix} \ddots & & & \iddots \\ & \tilde{H}_F^{(m-1,0)} & \tilde{H}_F^{(m-1,1)} & \tilde{H}_F^{(m-1,2)} \\ & \tilde{H}_F^{(m,-1)} & \tilde{H}_F^{(m,0)} & \tilde{H}_F^{(m,1)} \\ & \tilde{H}_F^{(m+1,-2)} & \tilde{H}_F^{(m+1,-1)} & \tilde{H}_F^{(m+1,0)} \\ \iddots & & & \ddots \end{bmatrix}, \tag{C24}$$

where

$$\tilde{H}_F^{(m,\kappa_m)} = \begin{bmatrix} \ddots & & & \iddots \\ & D_{m,l-1}^{\kappa_m,0} & D_{m,l-1}^{\kappa_m,1} & D_{m,l-1}^{\kappa_m,2} \\ & [D_{m,l}^{\kappa_m,-1}]^\dagger & D_{m,l}^{\kappa_m,0} & D_{m,l}^{\kappa_m,1} \\ & [D_{m,l+1}^{\kappa_m,-2}]^\dagger & [D_{m,l+1}^{\kappa_m,-1}]^\dagger & D_{m,l+1}^{\kappa_m,0} \\ \iddots & & & \ddots \end{bmatrix}. \tag{C25}$$

We can break the above Hamiltonian into diagonal and off-diagonal elements and consider all the off-diagonal elements as perturbation. However, there are many off-diagonal elements, and they will compete against each other. We first try to separate the most significant off-diagonal terms under different approximations and cancel those with negligible contributions. Let us start with the Hamiltonian with only one off-diagonal element:

$$\tilde{H}_F^{(0)} = \begin{bmatrix} \ddots & & & \iddots \\ & \tilde{H}_{F,0}^{(m-1,0)} & 0 & 0 \\ & 0 & \tilde{H}_{F,0}^{(m,0)} & 0 \\ & 0 & 0 & \tilde{H}_{F,0}^{(m+1,0)} \\ \iddots & & & \ddots \end{bmatrix}. \tag{C26}$$

Here

$$\tilde{H}_{F,0}^{(m,0)} = \begin{bmatrix} \ddots & & & \iddots \\ & D_{m,l-1}^{0,0} & 0 & 0 \\ & 0 & D_{m,l}^{0,0} & 0 \\ & 0 & 0 & D_{m,l+1}^{0,0} \\ \iddots & & & \ddots \end{bmatrix} \tag{C27}$$

with $D_{m,l}^{0,0}$ given by Eq. (C22).

Hamiltonian $\tilde{H}_F^{(0)}$ is a good approximation in the very-strong-driving regime, where $\Omega \gg \omega$. In the strong-driving regime, the two quasienergies will be separated by $(w_{\mathrm{q}}/2)J_0(\Omega\cos\nu/N_1\omega)J_0(\Omega\sin\nu/N_2\omega)$, which is the only off-diagonal element present in the Hamiltonian. However, when one of the drives becomes weaker, the higher-order $k > 0$ Bessel function becomes larger, and the contribution from other off-diagonal elements cannot be neglected. Next, we study the quasienergies when one of the drives is strong whereas the other is weak, i.e., $\nu \ll \pi/4$. Without loss of generality, we choose $m = l = 0$. Following Ref. [48], the Floquet Hamiltonian takes the form

$$\tilde{H}_{\mathrm{F}}^{(1)} = \begin{bmatrix} \tilde{H}_F^{(-1,0)} & \tilde{H}_F^{(-1,1)} \\ \tilde{H}_F^{(0,-1)} & \tilde{H}_F^{(0,0)} \end{bmatrix}, \tag{C28}$$

where only $m, l = 0$ or -1 contributions survive at resonance and all other contributions can be neglected. Furthermore, we have

$$\tilde{H}_F^{(m,\kappa_m)} = \begin{bmatrix} D_{m,-1}^{\kappa_m,0} & D_{m,-1}^{\kappa_m,1} \\ [D_{m,0}^{\kappa_m,-1}]^\dagger & D_{m,0}^{\kappa_m,0} \end{bmatrix}. \tag{C29}$$

Expanding the Floquet matrix, and using the notation $\tilde{J}_{k,1} = J_k(\Omega \cos\nu/N_1\omega)$ and $\tilde{J}_{k,2} = J_k(\Omega \sin\nu/N_2\omega)$, we obtain

$$\tilde{H}_{\mathrm{F}}^{(1)} = \begin{bmatrix} -\frac{b}{2}-(N_1+N_2)\omega & -\frac{w_q}{2}\tilde{J}_{0,1}\tilde{J}_{0,2} & 0 & 0 & 0 & \frac{w_q}{2}\tilde{J}_{1,1}\tilde{J}_{0,2} & 0 & \frac{w_q}{2}\tilde{J}_{1,1}\tilde{J}_{1,2} \\ -\frac{w_q}{2}\tilde{J}_{0,1}\tilde{J}_{0,2} & \frac{b}{2}-(N_1+N_2)\omega & 0 & 0 & -\frac{w_q}{2}\tilde{J}_{1,1}\tilde{J}_{0,2} & 0 & \frac{w_q}{2}\tilde{J}_{1,1}\tilde{J}_{1,2} & 0 \\ 0 & 0 & -\frac{b}{2}-N_1\omega & -\frac{w_q}{2}\tilde{J}_{0,1}\tilde{J}_{0,2} & 0 & \frac{w_q}{2}\tilde{J}_{1,1}\tilde{J}_{1,2} & 0 & \frac{w_q}{2}\tilde{J}_{1,1}\tilde{J}_{0,2} \\ 0 & 0 & -\frac{w_q}{2}\tilde{J}_{0,1}\tilde{J}_{0,2} & \frac{b}{2}-N_1\omega & \frac{w_q}{2}\tilde{J}_{1,1}\tilde{J}_{1,2} & 0 & -\frac{w_q}{2}\tilde{J}_{1,1}\tilde{J}_{0,2} & 0 \\ 0 & -\frac{w_q}{2}\tilde{J}_{1,1}\tilde{J}_{0,2} & 0 & \frac{w_q}{2}\tilde{J}_{1,1}\tilde{J}_{1,2} & -\frac{b}{2}-N_2\omega & -\frac{w_q}{2}\tilde{J}_{0,1}\tilde{J}_{0,2} & 0 & 0 \\ \frac{w_q}{2}\tilde{J}_{1,1}\tilde{J}_{0,2} & 0 & \frac{w_q}{2}\tilde{J}_{1,1}\tilde{J}_{1,2} & 0 & -\frac{w_q}{2}\tilde{J}_{0,1}\tilde{J}_{0,2} & \frac{b}{2}-N_2\omega & 0 & 0 \\ 0 & \frac{w_q}{2}\tilde{J}_{1,1}\tilde{J}_{1,2} & 0 & -\frac{w_q}{2}\tilde{J}_{1,1}\tilde{J}_{0,2} & 0 & 0 & -\frac{b}{2} & -\frac{w_q}{2}\tilde{J}_{0,1}\tilde{J}_{0,2} \\ \frac{w_q}{2}\tilde{J}_{1,1}\tilde{J}_{1,2} & 0 & \frac{w_q}{2}\tilde{J}_{1,1}\tilde{J}_{0,2} & 0 & 0 & 0 & -\frac{w_q}{2}\tilde{J}_{0,1}\tilde{J}_{0,2} & \frac{b}{2} \end{bmatrix}. \tag{C30}$$

In the fast-driving regime ($\omega \approx w_q$), the quasienergies are given by the Hamiltonian

$$\tilde{H}_{\mathrm{F}}^{(1)} = \begin{bmatrix} -\frac{b}{2}-(N_1+N_2)\omega & -\frac{w_q}{2}\tilde{J}_{0,1}\tilde{J}_{0,2} & 0 & \frac{w_q}{2}\tilde{J}_{1,1}\tilde{J}_{1,2} \\ -\frac{w_q}{2}\tilde{J}_{0,1}\tilde{J}_{0,2} & \frac{b}{2}-(N_1+N_2)\omega & \frac{w_q}{2}\tilde{J}_{1,1}\tilde{J}_{1,2} & 0 \\ 0 & \frac{w_q}{2}\tilde{J}_{1,1}\tilde{J}_{1,2} & -\frac{b}{2}-N_2\omega & -\frac{w_q}{2}\tilde{J}_{0,1}\tilde{J}_{0,2} \\ \frac{w_q}{2}\tilde{J}_{1,1}\tilde{J}_{1,2} & 0 & -\frac{w_q}{2}\tilde{J}_{0,1}\tilde{J}_{1,2} & \frac{b}{2}-N_2\omega \end{bmatrix}. \tag{C31}$$

Substituting $(N_1+N_2)\omega \to \omega$, we obtain the Floquet quasienergy gap

$$\Delta\epsilon = \omega - \{\Theta^2 + \omega^2 + w_q^2\tilde{J}_{1,1}^2\tilde{J}_{1,2}^2 - 2\Theta\omega\}^{1/2}, \tag{C32}$$

where we have defined $\Theta^2 = b^2 + w_q^2\tilde{J}_{0,1}^2\tilde{J}_{0,2}^2$. The above expression for the quasienergy gap agrees well with numerical results in the fast-driving regime, particularly when one drive is much weaker than the other ($\nu \ll \pi/4$). Notably, qualitative agreement persists even beyond this regime.

1. Multiphoton resonance: ac Stark shift and power broadening

Using Eq. (C24), the GVV Hamiltonian for the degeneracy condition $-b/2 \approx b/2 - mN_1\omega - lN_2\omega$ is given by [45]

$$H_{\mathrm{GVV}} = \begin{pmatrix} -b/2+\chi & -(w_q/2)\tilde{J}_{-m,1}\tilde{J}_{-l,2} \\ -(w_q/2)\tilde{J}_{-m,1}\tilde{J}_{-l,2} & b/2 - mN_1\omega - lN_2\omega - \chi \end{pmatrix}. \tag{C33}$$

To calculate the level shifts χ corresponding to the transition $|\phi_{00}^+\rangle$ to $|\phi_{-m,-l}^-\rangle$, we apply the nearly degenerate GVV perturbation method [45]. The 2×2 matrix $\mathcal{H}$ and its eigenstates ϕ can be expanded in powers of $-w_q/2$ as

$$\mathcal{H} = \sum_{k=0}^{\infty}(-w_q/2)^k\mathcal{H}^{(k)} \quad \text{and} \quad \phi = \sum_{k=0}^{\infty}(-w_q/2)^k\phi^{(k)}. \tag{C34}$$

Assuming that the states $|\phi_{00}^+\rangle$ to $|\phi_{-m,-l}^-\rangle$ are nearly degenerate, we have $-b/2 \approx b/2 - mN_1\omega - lN_2\omega$. Let the zeroth-order state $|\phi^{(0)}\rangle = \{\phi_+^{(0)}, \phi_-^{(0)}\}$, such that $\phi_+^{(0)} = |\phi_+^{00}\rangle$ and $\phi_-^{(0)} = |\phi_-^{-m,-l}\rangle$. The zeroth-order correction in $\mathcal{H}$ is then given by

$$\mathcal{H}^{(0)} = \begin{pmatrix} -b/2 & 0 \\ 0 & b/2 - mN_1\omega - lN_2\omega \end{pmatrix}. \tag{C35}$$

Now calculating the first-order terms in the expansion of $\mathcal{H}$ using the GVV method [45,49], we have

$$\mathcal{H}^{(1)} = \langle\phi^{(0)}|V'|\phi^{(0)}\rangle = \tilde{J}_{-m,1}\tilde{J}_{-l,2}\begin{pmatrix} 0 & 1 \\ 1 & 0 \end{pmatrix}. \tag{C36}$$

Further using the techniques in Ref. [45,49], we obtain

$$\phi_+^{(1)} = \sum_{\substack{j,k=-\infty \\ j,k\neq -m,-l}}^{+\infty} \frac{-\tilde{J}_{j,1}\tilde{J}_{k,2}}{(b + jN_1\omega + kN_2\omega)}|\phi_{jk}^-\rangle, \tag{C37}$$

$$\phi_{-}^{(1)} = \sum_{\substack{j,k=-\infty \\ j,k\neq -m,-l}}^{+\infty} \frac{\tilde{J}_{j,1}\tilde{J}_{k,2}}{(b+jN_1\omega+kN_2\omega)} |\phi^{+}_{-j-m,-k-l}\rangle, \quad \text{(C38)}$$

which we can use to compute the next-order corrections in $\mathcal{H}$ given by

$$\begin{aligned}\mathcal{H}^{(2)} &= \langle\phi^{(0)}|V'|\phi^{(1)}\rangle - \mathcal{H}^{(1)}\langle\phi^{(0)}|\phi^{(1)}\rangle \\ &= \sum_{\substack{j,k=-\infty \\ j,k\neq -m,-l}}^{+\infty} \frac{\tilde{J}^2_{j,1}\tilde{J}^2_{k,2}}{(b+jN_1\omega+kN_2\omega)} \begin{pmatrix}-1 & 0\\ 0 & 1\end{pmatrix}. \quad \text{(C39)}\end{aligned}$$

Now comparing the matrix structures in Eqs. (C36) and (C39) with Eq. (C33), we see that χ can be related to the odd powers of w_q/ω,

$$\chi = -\frac{w_q^2}{4} \sum_{\substack{j,k=-\infty \\ j,k\neq -m,-l}}^{+\infty} \frac{(\tilde{J}_{j,1})^2(\tilde{J}_{k,2})^2}{(b+jN_1\omega+kN_2\omega)} + \mathcal{O}\left(\frac{w_q}{\omega}\right)^3. \quad \text{(C40)}$$

[1] V. E. Manucharyan, J. Koch, L. I. Glazman, and M. H. Devoret, Fluxonium: Single Cooper-pair circuit free of charge offsets, Science **326**, 113 (2009).

[2] A. Grimm, N. E. Frattini, S. Puri, S. O. Mundhada, S. Touzard, M. Mirrahimi, S. M. Girvin, S. Shankar, and M. H. Devoret, Stabilization and operation of a Kerr-cat qubit, Nature **584**, 205 (2020).

[3] Y. Nakamura, Y. A. Pashkin, and J. Tsai, Coherent control of macroscopic quantum states in a single-Cooper-pair box, Nature **398**, 786 (1999).

[4] P. Krantz, M. Kjaergaard, F. Yan, T. P. Orlando, S. Gustavsson, and W. D. Oliver, A quantum engineer's guide to superconducting qubits, Appl. Phys. Rev. **6**, 021318 (2019).

[5] J. Koch, T. M. Yu, J. Gambetta, A. A. Houck, D. I. Schuster, J. Majer, A. Blais, M. H. Devoret, S. M. Girvin, and R. J. Schoelkopf, Charge-insensitive qubit design derived from the Cooper pair box, Phys. Rev. A **76**, 042319 (2007).

[6] L. B. Nguyen, Y. Kim, A. Hashim, N. Goss, B. Marinelli, B. Bhandari, D. Das, R. K. Naik, J. M. Kreikebaum, A. N. Jordan *et al.*, Programmable Heisenberg interactions between Floquet qubits, Nat. Phys. **20**, 240 (2024).

[7] B. Bhandari, I. Huang, A. Hajr, K. Yanik, B. Qing, K. Wang, D. I. Santiago, J. Dressel, I. Siddiqi, and A. N. Jordan, Symmetrically threaded superconducting quantum interference devices as next-generation Kerr-cat qubits, PRX Quantum **6**, 030338 (2025).

[8] A. Hajr, B. Qing, K. Wang, G. Koolstra, Z. Pedramrazi, Z. Kang, L. Chen, L. B. Nguyen, C. Jünger, N. Goss, I. Huang, B. Bhandari, N. E. Frattini, S. Puri, J. Dressel, A. N. Jordan, D. I. Santiago, and I. Siddiqi, High-coherence Kerr-cat qubit in 2D architecture, Phys. Rev. X **14**, 041049 (2024).

[9] A. Bechtold, D. Rauch, F. Li, T. Simmet, P.-L. Ardelt, A. Regler, K. Müller, N. A. Sinitsyn, and J. J. Finley, Three-stage decoherence dynamics of an electron spin qubit in an optically active quantum dot, Nat. Phys. **11**, 1005 (2015).

[10] G. Ithier, E. Collin, P. Joyez, P. J. Meeson, D. Vion, D. Esteve, F. Chiarello, A. Shnirman, Y. Makhlin, J. Schriefl, and G. Schön, Decoherence in a superconducting quantum bit circuit, Phys. Rev. B **72**, 134519 (2005).

[11] Q. Guo, S.-B. Zheng, J. Wang, C. Song, P. Zhang, K. Li, W. Liu, H. Deng, K. Huang, D. Zheng, X. Zhu, H. Wang, C.-Y. Lu, and J.-W. Pan, Dephasing-insensitive quantum information storage and processing with superconducting qubits, Phys. Rev. Lett. **121**, 130501 (2018).

[12] F. Yan, S. Gustavsson, J. Bylander, X. Jin, F. Yoshihara, D. G. Cory, Y. Nakamura, T. P. Orlando, and W. D. Oliver, Rotating-frame relaxation as a noise spectrum analyser of a superconducting qubit undergoing driven evolution, Nat. Commun. **4**, 2337 (2013).

[13] J. Jing, P. Huang, and X. Hu, Decoherence of an electrically driven spin qubit, Phys. Rev. A **90**, 022118 (2014).

[14] A. Y. Smirnov, Decoherence and relaxation of a quantum bit in the presence of Rabi oscillations, Phys. Rev. B **67**, 155104 (2003).

[15] A. Blais, A. L. Grimsmo, S. M. Girvin, and A. Wallraff, Circuit quantum electrodynamics, Rev. Mod. Phys. **93**, 025005 (2021).

[16] G. Q. AI and Collaborators, Quantum error correction below the surface code threshold, Nature **638**, 920 (2025).

[17] T. Kobayashi, J. Salfi, C. Chua, J. Van Der Heijden, M. G. House, D. Culcer, W. D. Hutchison, B. C. Johnson, J. C. McCallum, H. Riemann *et al.*, Engineering long spin coherence times of spin–orbit qubits in silicon, Nat. Mater. **20**, 38 (2021).

[18] G. Burkard, T. D. Ladd, A. Pan, J. M. Nichol, and J. R. Petta, Semiconductor spin qubits, Rev. Mod. Phys. **95**, 025003 (2023).

[19] N. W. Hendrickx, L. Massai, M. Mergenthaler, F. J. Schupp, S. Paredes, S. W. Bedell, G. Salis, and A. Fuhrer, Sweet-spot operation of a germanium hole spin qubit with highly anisotropic noise sensitivity, Nat. Mater. **23**, 920 (2024).

[20] M. D. Reed, B. M. Maune, R. W. Andrews, M. G. Borselli, K. Eng, M. P. Jura, A. A. Kiselev, T. D. Ladd, S. T. Merkel, I. Milosavljevic, E. J. Pritchett, M. T. Rakher, R. S. Ross, A. E. Schmitz, A. Smith, J. A. Wright, M. F. Gyure, and A. T. Hunter, Reduced sensitivity to charge noise in semiconductor spin qubits via symmetric operation, Phys. Rev. Lett. **116**, 110402 (2016).

[21] T. Tanttu, W. H. Lim, J. Y. Huang, N. Dumoulin Stuyck, W. Gilbert, R. Y. Su, M. Feng, J. D. Cifuentes, A. E. Seedhouse, S. K. Seritan *et al.*, Assessment of the errors of high-fidelity two-qubit gates in silicon quantum dots, Nat. Phys. **20**, 1804 (2024).

[22] F. Yoshihara, K. Harrabi, A. O. Niskanen, Y. Nakamura, and J. S. Tsai, Decoherence of flux qubits due to $1/f$ flux noise, Phys. Rev. Lett. **97**, 167001 (2006).

[23] L. B. Nguyen, Y.-H. Lin, A. Somoroff, R. Mencia, N. Grabon, and V. E. Manucharyan, High-coherence fluxonium qubit, Phys. Rev. X **9**, 041041 (2019).

[24] Z. Huang, P. S. Mundada, A. Gyenis, D. I. Schuster, A. A. Houck, and J. Koch, Engineering dynamical sweet spots to protect qubits from $1/f$ noise, Phys. Rev. Appl. **15**, 034065 (2021).

[25] S. M. Anton, C. Müller, J. S. Birenbaum, S. R. O'Kelley, A. D. Fefferman, D. S. Golubev, G. C. Hilton, H.-M. Cho, K. D. Irwin, F. C. Wellstood, G. Schön, A. Shnirman, and

J. Clarke, Pure dephasing in flux qubits due to flux noise with spectral density scaling as $1/f^{\alpha}$, Phys. Rev. B **85**, 224505 (2012).
[26] T. M. Hazard, A. Gyenis, A. Di Paolo, A. T. Asfaw, S. A. Lyon, A. Blais, and A. A. Houck, Nanowire superinductance fluxonium qubit, Phys. Rev. Lett. **122**, 010504 (2019).
[27] J. A. Valery, S. Chowdhury, G. Jones, and N. Didier, Dynamical sweet spot engineering via two-tone flux modulation of superconducting qubits, PRX Quantum **3**, 020337 (2022).
[28] N. Didier, E. A. Sete, J. Combes, and M. P. da Silva, ac flux sweet spots in parametrically modulated superconducting qubits, Phys. Rev. Appl. **12**, 054015 (2019).
[29] Y. Hajati and G. Burkard, Dynamic sweet spot of driven flopping-mode spin qubits in planar quantum dots, Phys. Rev. B **110**, 245301 (2024).
[30] J. R. Petta, A. C. Johnson, J. M. Taylor, E. A. Laird, A. Yacoby, M. D. Lukin, C. M. Marcus, M. P. Hanson, and A. C. Gossard, Coherent manipulation of coupled electron spins in semiconductor quantum dots, Science **309**, 2180 (2005).
[31] J. Medford, L. Cywiński, C. Barthel, C. M. Marcus, M. P. Hanson, and A. C. Gossard, Scaling of dynamical decoupling for spin qubits, Phys. Rev. Lett. **108**, 086802 (2012).
[32] J. T. Muhonen, J. P. Dehollain, A. Laucht, F. E. Hudson, R. Kalra, T. Sekiguchi, K. M. Itoh, D. N. Jamieson, J. C. McCallum, A. S. Dzurak *et al.*, Storing quantum information for 30 s in a nanoelectronic device, Nat. Nanotech. **9**, 986 (2014).
[33] N. Ezzell, B. Pokharel, L. Tewala, G. Quiroz, and D. A. Lidar, Dynamical decoupling for superconducting qubits: A performance survey, Phys. Rev. Appl. **20**, 064027 (2023).
[34] K. Viebahn, J. Minguzzi, K. Sandholzer, A.-S. Walter, M. Sajnani, F. Görg, and T. Esslinger, Suppressing dissipation in a Floquet-Hubbard system, Phys. Rev. X **11**, 011057 (2021).
[35] B. Qing, A. Hajr, K. Wang, G. Koolstra, L. B. Nguyen, J. Hines, I. Huang, B. Bhandari, Z. Padramrazi, L. Chen *et al.*, Kerr-cat qubit operations below the fault-tolerant threshold, arXiv:2411.04442.
[36] N. E. Frattini, R. G. Cortiñas, J. Venkatraman, X. Xiao, Q. Su, C. U. Lei, B. J. Chapman, V. R. Joshi, S. M. Girvin, R. J. Schoelkopf, S. Puri, and M. H. Devoret, Observation of pairwise level degeneracies and the quantum regime of the Arrhenius law in a double-well parametric oscillator, Phys. Rev. X **14**, 031040 (2024).
[37] H. Bluhm, S. Foletti, I. Neder, M. Rudner, D. Mahalu, V. Umansky, and A. Yacoby, Dephasing time of GaAs electron-spin qubits coupled to a nuclear bath exceeding 200 μs, Nat. Phys. **7**, 109 (2011).
[38] Y. Chen, Z. Zhu, and K. Viebahn, Mitigating higher-band heating in Floquet-Hubbard lattices via two-tone driving, Phys. Rev. A **112**, L021301 (2025).
[39] A. Kou, W. C. Smith, U. Vool, R. T. Brierley, H. Meier, L. Frunzio, S. M. Girvin, L. I. Glazman, and M. H. Devoret, Fluxonium-based artificial molecule with a tunable magnetic moment, Phys. Rev. X **7**, 031037 (2017).
[40] J. M. Martinis, S. Nam, J. Aumentado, K. M. Lang, and C. Urbina, Decoherence of a superconducting qubit due to bias noise, Phys. Rev. B **67**, 094510 (2003).
[41] H. Zhang, S. Chakram, T. Roy, N. Earnest, Y. Lu, Z. Huang, D. K. Weiss, J. Koch, and D. I. Schuster, Universal fast-flux control of a coherent, low-frequency qubit, Phys. Rev. X **11**, 011010 (2021).
[42] E. S. Fried, P. Sivarajah, N. Didier, E. A. Sete, M. P. da Silva, B. R. Johnson, and C. A. Ryan, Assessing the influence of broadband instrumentation noise on parametrically modulated superconducting qubits, arXiv:1908.11370.
[43] P. S. Mundada, A. Gyenis, Z. Huang, J. Koch, and A. A. Houck, Floquet-engineered enhancement of coherence times in a driven fluxonium qubit, Phys. Rev. Appl. **14**, 054033 (2020).
[44] N. Didier, Flux control of superconducting qubits at dynamical sweet spots, arXiv:1912.09416 [quant-ph].
[45] S.-K. Son, S. Han, and S.-I. Chu, Floquet formulation for the investigation of multiphoton quantum interference in a superconducting qubit driven by a strong ac field, Phys. Rev. A **79**, 032301 (2009).
[46] J. H. Shirley, Solution of the Schrödinger equation with a Hamiltonian periodic in time, Phys. Rev. **138**, B979 (1965).
[47] T.-S. Ho, S.-I. Chu, and J. V. Tietz, Semiclassical many-mode Floquet theory, Chem. Phys. Lett. **96**, 464 (1983).
[48] C. Deng, J.-L. Orgiazzi, F. Shen, S. Ashhab, and A. Lupascu, Observation of Floquet states in a strongly driven artificial atom, Phys. Rev. Lett. **115**, 133601 (2015).
[49] J. O. Hirschfelder, Almost degenerate perturbation theory, Chem. Phys. Lett. **54**, 1 (1978).